

Paper Microfluidics Goes Digital

Ryan Fobel, Andrea E. Kirby, Alphonsus H. C. Ng, Ramin R. Farnood, and Aaron R. Wheeler*

Paper microfluidics has recently emerged as simple and low-cost paradigm for fluid manipulation and diagnostic testing.^[1–3] Compared to traditional “lab-on-a-chip” technologies, it has several distinct advantages that make it especially suitable for point-of-care testing in low-resource settings. The most obvious benefits are the low cost of paper and the highly developed infrastructure of the printing industry, making production of paper-based devices both economical and scalable.^[3] Other important benefits include the ease of disposal, stability of dried reagents,^[4] and the reduced dependence on expensive external instrumentation.^[5,6]

While the paper microfluidics concept has transformative potential, this class of devices is not without drawbacks. Many assays have limited sensitivity in the paper format because of reduced sample volumes and limitations of colorimetric readouts.^[6] These devices also exhibit large dead volumes as the entire channel must be filled to drive capillary flow. But perhaps the most significant challenge for paper-based microfluidic devices is their passive nature, which makes it difficult to perform complex multiplexing and multistep assays (e.g., sandwich enzyme-linked immunosorbent assay (ELISA)). There has been progress in expanding device complexity through the development of three-dimensional channel networks^[7,8] and adapting channel length, width and matrix properties can provide control of reagent sequencing and time of arrival at specific points on the device.^[9] Active “valve” analogues have also been demonstrated using cut-out fluidic switches,^[10] and manual folding;^[11] however, these techniques require operator intervention which can introduce additional complications.

Some groups have implemented complicated, multistep assays including sandwich ELISA using paper “well plates” and manual pipetting.^[6,12–16] These assays are analogous to those performed in standard 96-well polystyrene plates, but the “plates” are pieces of paper patterned with hydrophobic/philic zones. The drawback to this class of devices is that they are not

truly “microfluidics” – unlike the methods described above, each reagent must be pipetted into a given well to implement an assay, similar to conventional multi-well plate techniques.

Here, we report an alternative approach for implementing fully automated, complex, multistep reactions on paper-based substrates: the first example of so-called “digital microfluidics” implemented on paper. Digital microfluidics (DMF) is a technology for manipulating nano-to-microliter-sized liquid drops on an array of electrodes using electric fields. Electrostatic forces can be used to merge, mix, split, and dispense drops from reservoirs, all without pumps or moving parts. While DMF has been applied to a wide range of applications,^[17] a significant challenge has been the lack of a scalable and economical method of device fabrication – most academic labs use photolithography in cleanroom facilities to form patterns of electrodes on glass and silicon. One scalable technique is the application of printed circuit board (PCB) fabrication to form DMF devices,^[18–20] but we propose that the new methods reported here, which rely on inkjet printing on paper, may offer superior performance and be better suited for rapid prototyping. Moreover, we suggest that the new device format described has the potential to combine the power and flexibility of DMF with the many benefits of paper-based microfluidics.

Paper DMF devices were formed by inkjet printing arrays of silver driving electrodes and reservoirs connected to contact pads onto paper substrates optimized for inkjet printing. The key requirements for paper used for this application are that it: i) exhibits a smooth surface, ii) provides a barrier to prevent ink from wicking into the fibers, and iii) has an appropriate surface energy. We have printed working DMF devices on a variety of commercially available inkjet photo papers (e.g., Epson Premium Photo Glossy and HP Premium Plus Photo Glossy), but we opted for a custom paper^[21] for the bulk of the work reported here because it has a known composition and will allow for future optimization and control of its properties. **Figure 1a** and **b** contain representative photographs of the two designs of devices formed on paper. In practice, each paper substrate formed a device bottom plate, which was joined with a conductive top plate to manipulate 400–800 nL drops sandwiched between them (Figure S1, Supporting Information).

A key feature for forming digital microfluidic devices is the spatial resolution, as adjacent electrodes separated by large gaps (>100 μm) are problematic for drop movement.^[22] A resolution test pattern in Figure 1c demonstrates horizontal and vertical feature capabilities as small as 30 μm . In general, we observed that larger features had a lower probability of failure caused by electrical shorts or breaks, so the driving electrodes in the paper DMF devices used here were spaced between 60–90 μm from each other. In contrast, typical PCB manufacturing processes cannot produce features smaller than 100 μm . Another key

R. Fobel, A. H. C. Ng, Prof. A. R. Wheeler
Institute for Biomaterials and Biomedical Engineering
University of Toronto
164 College St., Toronto, ON M5S 3E1, Canada
E-mail: aaron.wheeler@utoronto.ca

A. E. Kirby, Prof. A. R. Wheeler
Department of Chemistry,
University of Toronto
80 St George St., Toronto, ON M5S 3H6, Canada

Prof. R. R. Farnood
Department of Chemical Engineering and Applied Chemistry,
University of Toronto
200 College Street, Toronto, ON M5S 3E5, Canada



DOI: 10.1002/adma.201305168

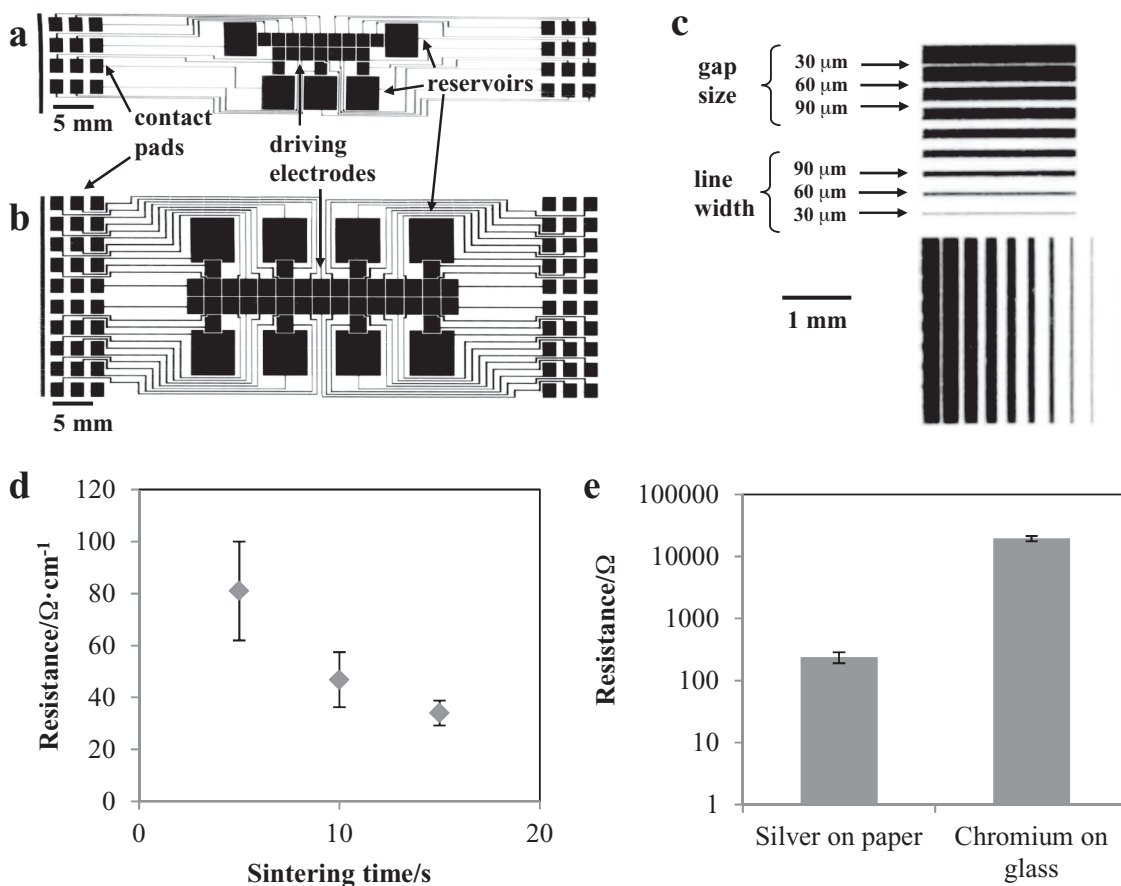


Figure 1. Characterization of printing resolution and conductivity. a,b) Photos of paper DMF devices patterned with Design A (a) and Design B (b). c) Photo of printed test pattern showing gradients of line/gap widths in horizontal and vertical directions. d) Effect of sintering time on the resistance of 150 μm wide printed silver traces. e) Average resistance of all traces for DMF device Design A fabricated by inkjet (silver on paper) and by standard photolithography (chromium on glass). Error bars are ± 1 standard deviation.

feature is conductivity – thin electrodes with poor conductivity can result in Joule heating and/or unplanned voltage drops. As shown in Figure 1d, inkjet printed trace resistance decreases as a function of sintering time. Sintering for ≥ 15 s caused a slight browning of the paper (which did not seem to affect function), so in the work described below, all devices were sintered for 10 s. Figure 1e shows that the printed traces were found to have resistances that were 500 times lower than those for devices with identical designs fabricated by standard photolithographic methods (i.e., chromium on glass). This difference in conductivity can be explained by differences in the bulk conductivity of silver versus chromium and the relative thickness of the metal layers (ca. 100 nm for chromium on glass and ca. 500 nm for silver on paper).

A third key feature for DMF devices is surface topography: shape and roughness. We use “shape” to refer to the topographical pattern arising from differences in height between electrodes and the gaps between them (i.e., “trenches” with depth defined by the thickness of the conductive/electrode layer), and “roughness” to refer to random variations in surface topography. The effects of surface topography for glass DMF devices bearing metal electrodes patterned by photolithography

(often used in academic labs) are negligible; in contrast, the performance of DMF devices formed by PCB fabrication can be severely compromised by topography.^[22]

Scanning electron microscopy (SEM) was used to evaluate the surface shape of the paper devices used here (Figure 2a,b). As shown, the thickness of the silver layer on inkjet printed paper devices is < 500 nm, which is much thinner than the 10–30 μm thick electrodes commonly found on devices formed from PCBs (note that deep “trenches” between electrodes on PCB-based DMF devices have been reported to be problematic for drop movement^[19,20,22]). Atomic force microscopy (AFM) was used to evaluate surface roughness, revealing a surface roughness (R_a) of $R_a \approx 250$ nm for bare silver on paper substrates, and $R_a < 100$ nm for silver-paper substrates after deposition of Parylene-C and Teflon. These values are between one and two orders of magnitude smaller than those reported for PCB DMF devices.^[18–20] The most straightforward measure of the effects of surface topography on DMF performance is to evaluate the actuation of individual drops. Figure 2c and 2d demonstrate the movability of water drops on paper devices. The instantaneous velocities of drops of water were measured by impedance sensing^[23] and the data suggests that the performance of paper

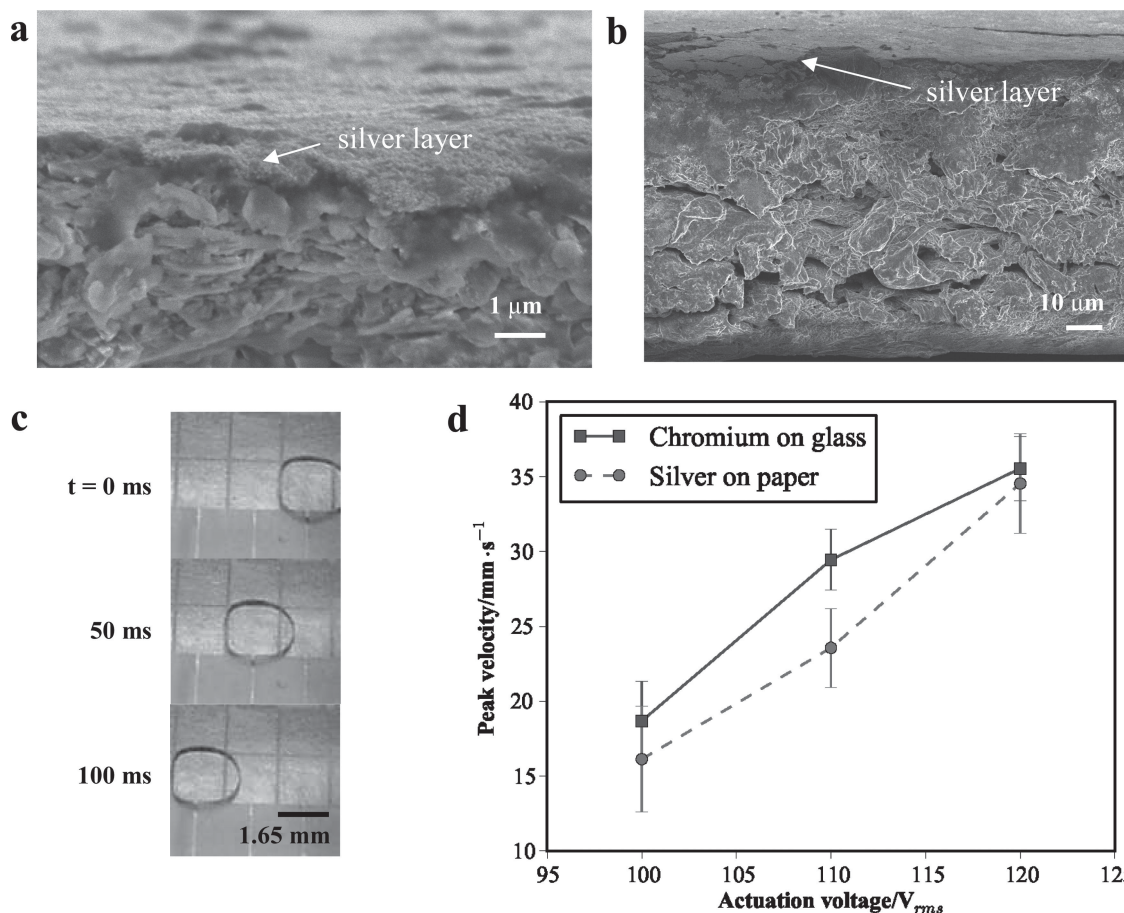


Figure 2. Surface topology and drop velocity (Design A). a,b) SEM images showing cross-sectional views of a paper device with a printed silver electrode. c) Series of video frames demonstrating translation of a drop of water on a paper device. d) Peak velocities of water drops on a paper DMF device (green circles) relative to those on a standard device fabricated by photolithography (blue squares). Error bars are ± 1 standard deviation.

DMF devices is comparable to that of glass devices formed by photolithography. In other words, paper DMF devices exhibit nearly identical performance to glass devices, a remarkable observation given the differences in fabrication (inkjet printing relative to lithography and etching in a cleanroom).

To date, we have fabricated more than one hundred working paper DMF devices. The devices are inexpensive and fast to make; e.g., the cost of ink and paper to form one device (Design A) is less than \$0.05 (see the online supplementary information), and the device can be printed in approximately 1 minute. We expect both cost and speed will improve dramatically as the printed electronics field matures and/or if these methods are scaled to larger production runs because: i) commercial conductive inks are still relatively expensive when ordered in small quantities; and ii) typical office inkjet printers (which rely on the same piezoelectric principle) have >100 nozzles compared to ≤ 6 that were practical to use simultaneously in this study. Since printing time is inversely proportional to the number of nozzles, we expect that in the future it may be possible to reduce this time to just seconds per device. Most importantly, the new paper substrates have the capacity to implement complex, multistep assays, representing an important new frontier for paper microfluidics.

Two tests were developed to probe the capacity of paper DMF devices for performing complex, multistep assays. As a first test, we explored the ability to generate an on-chip serial dilution and calibration curve for a homogeneous chemiluminescence assay: horseradish peroxidase (HRP) mixed with luminol/ H_2O_2 . As depicted in **Figure 3a**, this experiment requires 63 discrete steps: 27 dispense, 18 mix, 6 split, and 12 measure. From a total of three initial pipette steps, a four-point calibration curve can be created in less than 1 h. Despite this complexity, the assay was straightforward to implement reproducibly on paper DMF devices (**Figure 3b**, $R^2 = 0.993$). The complexity of this assay is such that it would likely be difficult or perhaps impossible to perform on a capillary-driven paper device.

As a second test to probe the feasibility of complex assay development using paper DMF and to demonstrate the suitability of these devices for low-cost diagnostic testing, we chose to implement a proof-of-principle rubella IgG sandwich ELISA. Rubella, also known as German measles, is a disease caused by the rubella virus. Although it poses few complications when acquired post-natally, congenital rubella syndrome can cause serious developmental defects including blindness, deafness and termination of pregnancy.^[24] As far as we are aware, this is

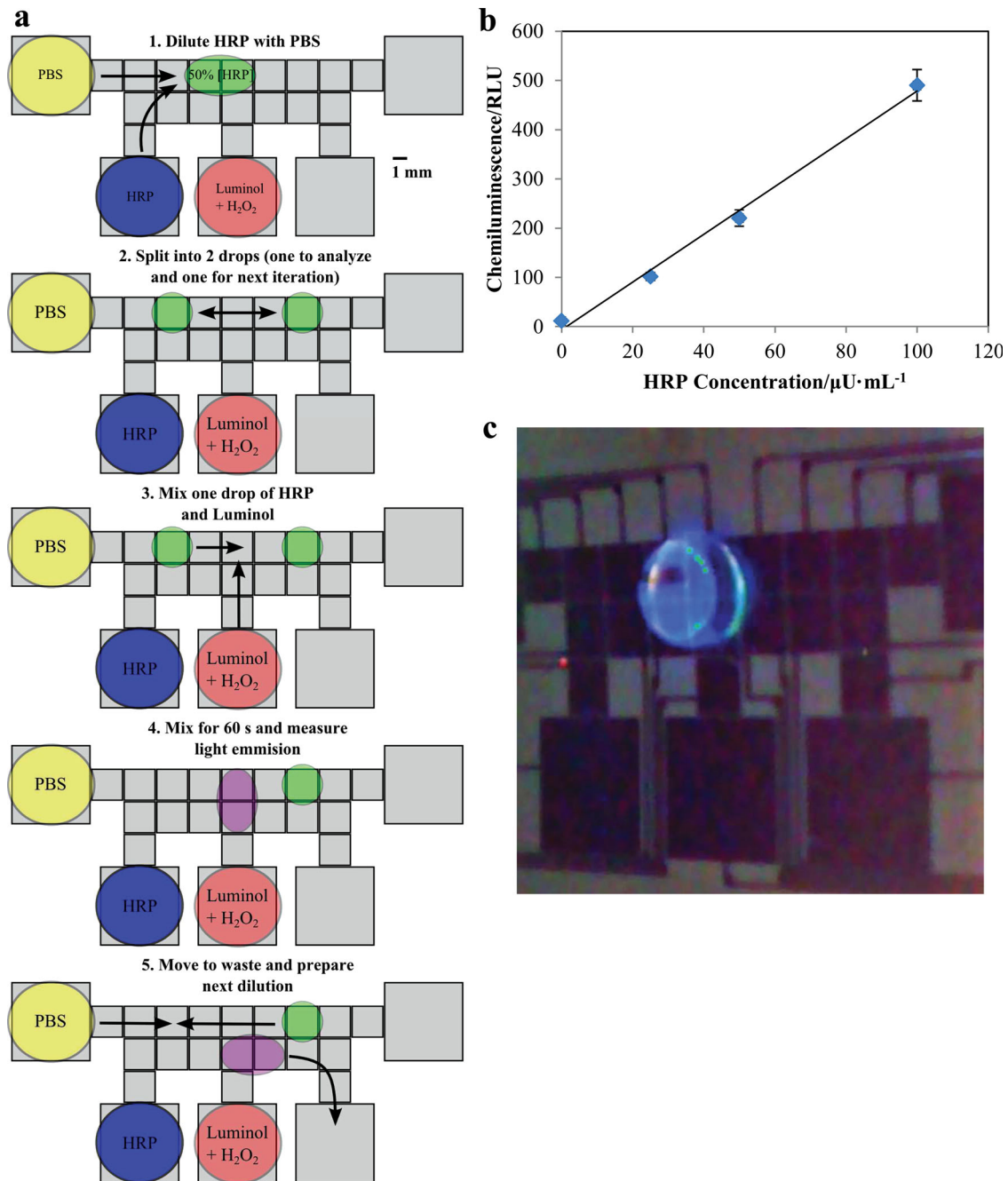


Figure 3. Homogeneous chemiluminescence assay generated on a paper DMF device (Design A) through on-chip serial dilution of HRP mixed with luminol/ H_2O_2 . a) Cartoon showing individual steps in the assay. b) Calibration curve; error bars are ± 1 standard deviation (some error bars are obscured by the data markers). c) Picture of a device after step 4 with top plate removed for visualization.

the first report of an assay for rubella IgG using a microfluidic device of any format.

The ELISA for rubella IgG required a larger electrode array, the use of magnetic-bead-linked inactivated rubella virus, and a motorized magnet for separation and washing^[25] (Figure 4a). 30 discrete steps were required for each concentration evaluated (11 dispense, 10 mix, 8 magnetic separation, and 1 measure), taking approximately 10 min. Most importantly, as shown in Figure 4b, the method was reproducible ($R^2 = 0.988$) and

sensitive (limit of detection = 0.15 IU/mL), demonstrating the ability to detect concentrations well below the 10 IU/mL clinical threshold.^[26] The inset in Figure 4b shows the immunocomplex for the assay. Note that unlike conventional ELISAs which use a capture antibody specific to a target analyte, in this case, the beads are coated with an inactivated virus and the primary antibody (rubella IgG) is the analyte. Sandwich ELISAs in a more traditional format (with antibodies immobilized on beads) have been performed on DMF devices with similar geometries

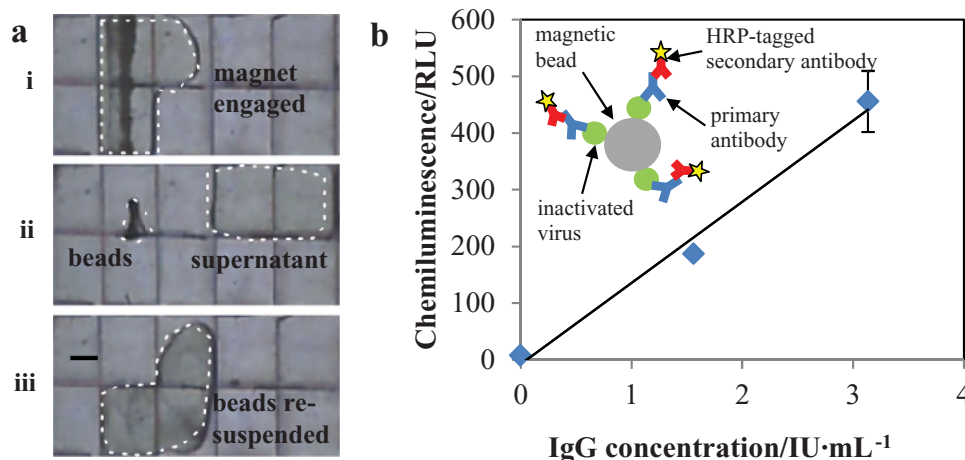


Figure 4. Rubella IgG immunoassay performed on a paper DMF device (Design B) with a luminol/H₂O₂ chemiluminescent readout. a) Still frames from a video sequence showing magnetic separation of beads from the supernatant and re-suspension in wash buffer. b) Calibration curve; error bars are ± 1 standard deviation (some error bars are obscured by the data markers). The inset shows the immunocomplex for the assay: a magnetic bead coated with inactivated virus, the primary antibody (rubella IgG) and the HRP-tagged secondary antibody.

formed in glass,^[25,27] so we propose that paper DMF will likely be compatible with ELISAs in a variety of formats. Furthermore, since magnetic beads are commercially available for a wide variety of antibodies, we expect that this procedure can provide a general blueprint toward quantifying a broad range of interesting biomarkers. In addition to the obvious benefit of low device cost, this method retains high analytical performance with greatly reduced sample volumes relative to conventional automated immunoassay analyzers.^[25,27]

Compared with traditional, capillary-driven paper microfluidics, the DMF format presents obvious tradeoffs. In cases where capillary-driven flow is sufficient, the additional complexity and cost of the required DMF instrumentation may be unwarranted. However, we note that the added costs for DMF are modest (e.g., an open-source DMF control system can be reproduced for a few thousand dollars^[23]) and they represent a one-time investment. Thus, we propose that for applications requiring flexibility and/or precise control of multistep reactions (e.g., a quantitative standard dilution curve for a sandwich ELISA), these added costs are justified. Opportunities for reducing the instrumentation costs (e.g., electrochemical readout^[28]) coupled with the low cost of the paper DMF consumables means that over the instrument lifetime, the cost per test can be made very low.

In conclusion, we have demonstrated the fabrication of DMF devices on paper using inkjet printing. We propose that this advance significantly extends the range of applications that can be easily implemented using paper-based microfluidics and is especially well-suited for complex, automated, multistep assays that would be difficult to perform with capillary-driven techniques. In the future, DMF fluid manipulation may be combined with capillary wetting features, thereby creating a form of paper "hybrid" devices that take advantage of the unique capabilities of both formats. In addition, the fabrication technique described here may be scaled to a roll-to-roll process^[21,29] for commercial production of low-cost DMF devices, or alternatively, this method may appeal to researchers interested in rapid prototyping of new DMF device designs.

Experimental Section

Reagents and Materials: Unless otherwise specified, reagents were purchased from Sigma-Aldrich (Oakville, ON). Deionized (DI) water had a resistivity of 18 M Ω cm at 25 °C. Pluronic L64 (BASF Corp., Germany) was generously donated by Brenntag Canada (Toronto, ON). Most paper substrates used for device printing were graciously provided by Prof. M. Toivakka of Åbo Akademi University, Finland;^[21] other substrates were from Epson (Premium Photo Glossy) and HP (Premium Plus Photo Glossy). On-chip reagent solutions were either obtained from vendors or were custom-made in-house. Reagents from vendors include rubella IgG standards and rubella-virus-coated paramagnetic microparticles from Abbott Laboratories (Abbott Park, IL), and SuperSignal ELISA Femto chemiluminescent substrate, comprising stable peroxide (H₂O₂) and Luminol-Enhancer solution, from Thermo Fischer Scientific (Rockford, IL). Custom DMF-compatible wash buffer and conjugate diluent were prepared as described previously.^[25,27] Prior to use, rubella IgG standards diluted in Dulbecco's phosphate-buffered saline (DPBS) containing 4% bovine serum albumin (BSA) and chemiluminescent substrate were supplemented with Pluronic L64 at 0.05% and 0.025% v/v, respectively to reduce protein adsorption and limit cross-contamination.^[30] Conjugate working solutions were formed by diluting horse-radish peroxidase (HRP) conjugated goat polyclonal Anti-Human IgG (16 ng/mL) in conjugate diluent. The microparticle working suspension was formed by pelleting, washing, and resuspending microparticles in Superblock Tris-buffered saline from Thermo Fischer Scientific (Rockford, IL) at ca. 1.5×10^8 particles/mL.

DMF Device Fabrication, Characterization, and Operation: DMF bottom plates were formed by printing electrode patterns onto paper substrates using a Dimatix DMP-2800 inkjet printer (FUJIFILM Dimatix, Inc., Santa Clara, CA) and SunTronic U6503 silver nanoparticle-based ink according to the manufacturer's instructions.

Briefly, the "Dimatix Model Fluid 2 Waveform" was used to drive the printhead at a voltage of 20–22 V with the cartridge at room temperature and an applied meniscus vacuum of 4–5 inches of H₂O. After printing, the substrates were sintered using a 1500 W infrared lamp^[29] at a distance of ca. 1 cm for 10 s. Two different device design patterns were used: Design A includes 5 reservoir electrodes (4.17 mm \times 4.17 mm) and 19 driving electrodes (1.65 mm \times 1.65 mm) and Design B includes 8 reservoir electrodes (5.6 mm \times 5.6 mm) and 38 driving electrodes (2.16 mm \times 2.16 mm). Design A was also fabricated from chromium on glass substrates (with chromium thickness \approx 100 nm) as described previously.^[23] Design B was used for the rubella IgG immunoassay assay while Design A was used for all other experiments. Paper substrates were

affixed to glass slides to ease handling. Teflon thread seal tape (McMaster-Carr, Cleveland, OH) was wrapped around the electrical contact pads to prevent them from being covered by subsequent insulating layers. Both types of substrates (glass and paper) were coated with 6.2 μm of Parylene-C in a vapor deposition instrument (Specialty Coating Systems, Indianapolis, IN) and ca. 50 nm of Teflon-AF 1600 (DuPont, Wilmington, DE) by spin-coating (1% wt/wt in Fluorinert FC-40, 1000 rpm, 30 s) and postbaking at 160 °C for 10 min. Indium tin oxide (ITO)-coated glass plates (Delta Technologies Ltd., Stillwater, MN) were also coated with 50 nm of Teflon-AF (as above) for use as device top plates. Top and bottom plates were joined by stacking two pieces of double-sided tape (ca. 80 μm ea.), resulting in a unit drop volume (covering a single driving electrode) of ca. 440 nL (Design A) and ca. 750 nL (Design B). Reagent reservoirs were filled by pipetting the reagent adjacent to the gap between the bottom and top plates and applying a driving potential to a reservoir electrode. The conductivity across 2 cm long/150 μm traces of inkjet printed silver on paper (after sintering for 5, 10, or 15 s) was measured with a Fluke 179 True RMS Digital Multimeter; 9 traces were evaluated for each condition (3 on 3 separate devices). The resistance between contact pads and driving electrodes was measured for all electrodes of Design A for 3 paper and 3 chromium on glass devices. These traces varied between 1–3 cm long and 100–150 μm wide, and the trace designs were identical for both paper and glass device formats. SEM images were acquired with a S-3400N Variable Pressure SEM (Hitachi High Technologies America, Inc., Schaumburg, IL) in secondary electron mode with an accelerating voltage of 5 kV. Surface roughness estimates are based on the arithmetic average of absolute height values across a 125 μm \times 125 μm window (512 \times 512 samples) measured in air with a Digital Instruments Nanoscope IIIA multimode AFM (Bruker Nano Surface, Santa Barbara, CA) in tapping mode (1 Hz scan rate). All images were subjected to a zero-order flatten and 2nd-order plane fit filters prior to analysis. Devices were interfaced through pogo-pin connectors to one of two variations of the open-source DropBot drop controller, either with^[25] or without^[23] integrated magnetic control and integrated PMT. Electrodes were switched using solid-state relays and velocities were measured using an impedance-based feedback circuit.^[23]

Homogeneous Chemiluminescence Assay: Drops of HRP standard (100 $\mu\text{U}/\text{mL}$ in DPBS supplemented with 0.05% v/v L64) and drops of wash buffer were dispensed from reservoirs, mixed, and merged to form a dilution series (1 \times , 2 \times , 4 \times). One drop of SuperSignal chemiluminescent substrate was then dispensed, mixed, and merged with each diluted drop of HRP, and the pooled drop was mixed for 60 s, driven to the detection area, and the emitted light was measured after 2 min with an H10682–110 PMT (Hamamatsu Photonics K.K., Hamamatsu, Japan). Each condition was repeated 3 times.

Rubella IgG Immunoassay: Using DMF magnetic separation for reagent exchange and particle washing as described previously,^[25] immunoassays were implemented in seven steps: i) A ca. 1.6 μL drop (2 unit volumes) containing paramagnetic particles was dispensed from a reservoir and separated from the diluent. ii) One drop of rubella IgG standard (0, 1.56 or 3.125 IU/mL) was dispensed, delivered to the immobilized particles, and mixed for 3 min. iii) The particles were washed three times in wash buffer and separated from the supernatant. iv) One drop of HRP conjugate solution was dispensed, delivered to the immobilized particles, and mixed for 2 min. v) The particles were washed three times in wash buffer. vi) The particles were separated from the wash buffer and resuspended in one drop of H_2O_2 , and this drop was merged and mixed with one drop of luminol-enhancer solution. vii) The pooled drop was incubated for 2 min and the chemiluminescent signal was recorded using the PMT. Each condition was repeated 2 times. The limit of detection was calculated as the concentration corresponding to the position on the curve of the average signal generated from blank measurements plus three times the standard deviation of the blank measurements.

Supporting Information

Supporting Information is available from the Wiley Online Library or from the author.

Acknowledgements

The authors thank the National Science and Engineering Research Council (NSERC) for funding this project and for fellowships for R.F., A.E.K., and A.H.C.N. A.R.W. thanks the Canada Research Chair (CRC) program for a CRC. The authors thank Prof. M. Toivakka of Åbo Akademi University, Finland for supplying paper samples, Abbott Diagnostics for supplying virus-bound particles and other reagents, and Prof. Chris Yip of the University of Toronto for assisting with the AFM measurements.

Received: October 17, 2013

Revised: November 29, 2013

Published online: January 23, 2014

- [1] A. W. Martinez, S. T. Phillips, M. J. Butte, G. M. Whitesides, *Angew. Chem. Int. Ed.* **2007**, *46*, 1318.
- [2] W. Zhao, A. van den Berg, *Lab Chip* **2008**, *8*, 1988.
- [3] X. Li, D. R. Ballerini, W. Shen, *Biomicrofluidics* **2012**, *6*, 011301.
- [4] G. E. Fridley, H. Q. Le, E. Fu, P. Yager, *Lab Chip* **2012**, *12*, 4321.
- [5] A. W. Martinez, S. T. Phillips, E. Carrilho, S. W. Thomas, H. Sindi, G. M. Whitesides, *Anal. Chem.* **2008**, *80*, 3699.
- [6] C.-M. Cheng, A. W. Martinez, J. Gong, C. R. Mace, S. T. Phillips, E. Carrilho, K. A. Mirica, G. M. Whitesides, *Angew. Chem. Int. Ed.* **2010**, *49*, 4771.
- [7] A. W. Martinez, S. T. Phillips, G. M. Whitesides, *Proc. Natl. Acad. Sci. USA* **2008**, *105*, 19606.
- [8] H. Liu, R. M. Crooks, *J. Am. Chem. Soc.* **2011**, *133*, 17564.
- [9] E. Fu, B. Lutz, P. Kauffman, P. Yager, *Lab Chip* **2010**, *10*, 918.
- [10] X. Li, J. Tian, T. Nguyen, W. Shen, *Anal. Chem.* **2008**, *80*, 9131.
- [11] A. V. Govindarajan, S. Ramachandran, G. D. Vigil, P. Yager, K. F. Böhringer, *Lab Chip* **2011**, *12*, 174.
- [12] J. Tian, X. Li, W. Shen, *Lab Chip* **2011**, *11*, 2869.
- [13] J. Yan, L. Ge, X. Song, M. Yan, S. Ge, J. Yu, *Chem. Eur. J.* **2012**, *18*, 4938.
- [14] S. Wang, L. Ge, X. Song, J. Yu, S. Ge, J. Huang, F. Zeng, *Biosens. Bioelectron.* **2012**, *31*, 212.
- [15] S. Wang, L. Ge, X. Song, M. Yan, S. Ge, J. Yu, F. Zeng, *Analyst* **2012**, *137*, 3821.
- [16] J. Yan, M. Yan, L. Ge, J. Yu, S. Ge, J. Huang, *Chem. Commun.* **2013**, *49*, 1383.
- [17] K. Choi, A. H. C. Ng, R. Fobel, A. R. Wheeler, *Annu. Rev. Anal. Chem.* **2012**, *5*, 413.
- [18] P. Y. Paik, V. K. Pamula, M. G. Pollack, K. Chakrabarty, in *Proc. Int. Conf. MicroTAS*, Transducer Research Foundation, San Diego, CA, USA **2005**, pp. 566–568.
- [19] J. Gong, C. J. Kim, in *Proc. IEEE MEMS*, Miami, Florida **2005**, pp. 726–729.
- [20] M. Abdelgawad, A. R. Wheeler, *Adv. Mater.* **2007**, *19*, 133.
- [21] R. Bollström, A. Määttänen, D. Tobjörk, P. Ihalainen, N. Kaihovirta, R. Österbacka, J. Peltonen, M. Toivakka, *Org. Electron.* **2009**, *10*, 1020.
- [22] M. Abdelgawad, A. Wheeler, *Microfluid. Nanofluid.* **2008**, *4*, 349.
- [23] R. Fobel, C. Fobel, A. R. Wheeler, *Appl. Phys. Lett.* **2013**, *102*, 193513.
- [24] J. Banatvala, D. Brown, *Lancet* **2004**, *363*, 1127.
- [25] K. Choi, A. H. C. Ng, R. Fobel, D. A. Chang-Yen, L. E. Yarnell, E. L. Pearson, C. M. Oleksak, A. T. Fischer, R. P. Luoma, J. M. Robinson, J. Audet, A. R. Wheeler, *Anal. Chem.* **2013**, *85*, 9638–9646.
- [26] L. P. Skendzel, *Am. J. Clin. Pathol.* **1996**, *106*, 170.
- [27] A. H. C. Ng, K. Choi, R. P. Luoma, J. M. Robinson, A. R. Wheeler, *Anal. Chem.* **2012**, *84*, 8805.
- [28] M. H. Shamsi, K. Choi, A. H. C. Ng, A. R. Wheeler, *Lab Chip* **2014**, *14*, 547–554.
- [29] D. Tobjörk, H. Aarnio, P. Pulkkinen, R. Bollström, A. Määttänen, P. Ihalainen, T. Mäkelä, J. Peltonen, M. Toivakka, H. Tenhu, R. Österbacka, *Thin Solid Films* **2012**, *520*, 2949.
- [30] S. H. Au, P. Kumar, A. R. Wheeler, *Langmuir* **2011**, *27*, 8586.